Comparison of Discontinuous Galerkin Formulations for the Acoustic Conservation Laws

Johannes Heinz[1], Manfred Kaltenbacher[2]

[1] TU Wien, Institute of Mechanics and Mechatronics, 1060 Vienna, Austria, Email: johannes.heinz@tuwien.ac.at

[2] TU Graz, Institute of Fundamentals and Theory in Electrical Engineering, 8010 Graz, Austria, Email: manfred.kaltenbacher@tugraz.at

Introduction

The VRACE ETN[1] aims, amongst others, to develop models which render high-quality audio for virtual reality applications in real-time on affordable hardware. Propagating waves spread from vibrating surfaces that generally do not oscillate harmonically. Thus, transient simulations, which take velocities as boundary conditions (BCs), are required.

Different methods for solving the acoustic conservation laws have been defined to date. The classical mixed formulation requires the acoustic pressure in L^2 and the acoustic particle velocity in $H(\mathrm{div})$; this naturally enforces continuous fluxes along element normals [2]. However, constructing higher-order $H(\mathrm{div})$ elements is a challenging endeavor, and their evaluation is computationally expensive [3]. Therefore, [2] suggests using the acoustic pressure in H^1 and the acoustic particle velocity in L^2; a Piola mapping enforces flux continuity on a discrete level. Using L^2 spaces for both variables yields discontinuous Galerkin (DG) methods; these methods are very attractive due to their properties regarding stability and efficiency [5]. DG schemes double all degrees of freedom on element faces; what seems to be a drawback regarding efficiency, at first sight, turns out to be a significant advantage. The mass matrix of the whole system of equations gets block diagonal, making it possible to compute its exact inverse extremely fast. Explicit time-stepping schemes for linear systems of equations are especially attractive in this setting since it involves only the inverse of the mass matrix and standard matrix-vector products. To get an overall fast and memory-efficient method, we do not assemble a global system matrix; instead, we use assembly-free operator applications, which is preferable on state-of-the-art hardware, see, e.g., in the context of DG methods [8].

Suitable numerical fluxes can improve the stability of DG discretizations. A standard approach is to use a central flux in combination with jump penalty terms [5]. Nguyen *et al.* and Kronbichler *et al.* [11, 7] penalize the acoustic pressure with the acoustic particle velocity and vice versa in the context of hybridizable DG formulations; resulting fluxes are known as Lax–Friedrichs fluxes. LeVeque *et al.* [9] derive a finite volume formulation by solving the Riemann problem. Based on this derivation, the corresponding DG formulation is derived in [6]; it turns out to be equivalent to the use of a Lax–Friedrichs flux. Zhang *et al.* [13] employ the local discontinuous Galerkin (LDG) method using generalized alternating numerical fluxes in the one-dimensional case. This can be seen as an upwinding scheme, written in penalty form. The penalty form has several advantages; amongst others, the amount of upwinding can be specified easily [1]. Exploiting this property leads to upwind-biased fluxes, which are discussed for time-dependent linear hyperbolic equations in [10]. The upwinding directions for the acoustic pressure and acoustic particle velocity are chosen opposite to ensure stability and symmetric operations.

Lax–Friedrichs fluxes and LDG fluxes (in case of 1D monotone upwind fluxes) have been shown to yield optimal rates of convergence in space by [11, 7] and [13], respectively. To the best of the authors' knowledge, no direct comparison of both methods has been provided in the literature for the acoustic conservation laws. Within this work, we compare both methods regarding accuracy and stability in 2D.

[1] https://vrace-etn.eu

Governing Equations

We are solving the acoustic wave equation in the form of a first-order system, also known as the wave equation in pressure-velocity form or the acoustic conservation laws. In a domain $\Omega \subset \mathbb{R}^d$ of dimension d and in a time interval $[0, T]$ they read

$$\rho \frac{\partial \boldsymbol{u}}{\partial t} + \nabla p = 0 \quad \text{in } \Omega \times [0,T], \tag{1}$$

$$\frac{1}{c^2}\frac{\partial p}{\partial t} + \rho \nabla \cdot \boldsymbol{u} = f \quad \text{in } \Omega \times [0,T], \tag{2}$$

$$\boldsymbol{u} = \boldsymbol{g}_u \quad \text{on } \partial\Omega_u. \tag{3}$$

Here p is the acoustic pressure, c is the speed of sound, and ρ the density of the underlying fluid. Within these equations, the acoustic particle velocity $\boldsymbol{u}$ occurs which makes it possible to introduce given velocities $\boldsymbol{g}_u$ at corresponding boundaries $\partial\Omega_u$ without any problems.

Spatial Discretization

To get to the discrete system, we follow the standard approach for DG methods (cf. [5]). We multiply the equations by the test functions $\boldsymbol{w}_h$ and q_h and integrate over the computational domain Ω_h, which consists of non-overlapping elements e of volume Ω^e. Corresponding broken polynomial spaces of needed test and trial functions are

$$\mathcal{V}_h^u = \left\{ \boldsymbol{u}_h \in [L_2(\Omega_h)]^d : \boldsymbol{u}_h|_{\Omega^e} \in [\mathcal{P}_{k_u}(\Omega^e)]^d, \forall e \right\}, \tag{4}$$

$$\mathcal{V}_h^p = \left\{ p_h \in L_2(\Omega_h) : p_h|_{\Omega^e} \in \mathcal{P}_{k_p}(\Omega^e), \forall e \right\}, \tag{5}$$

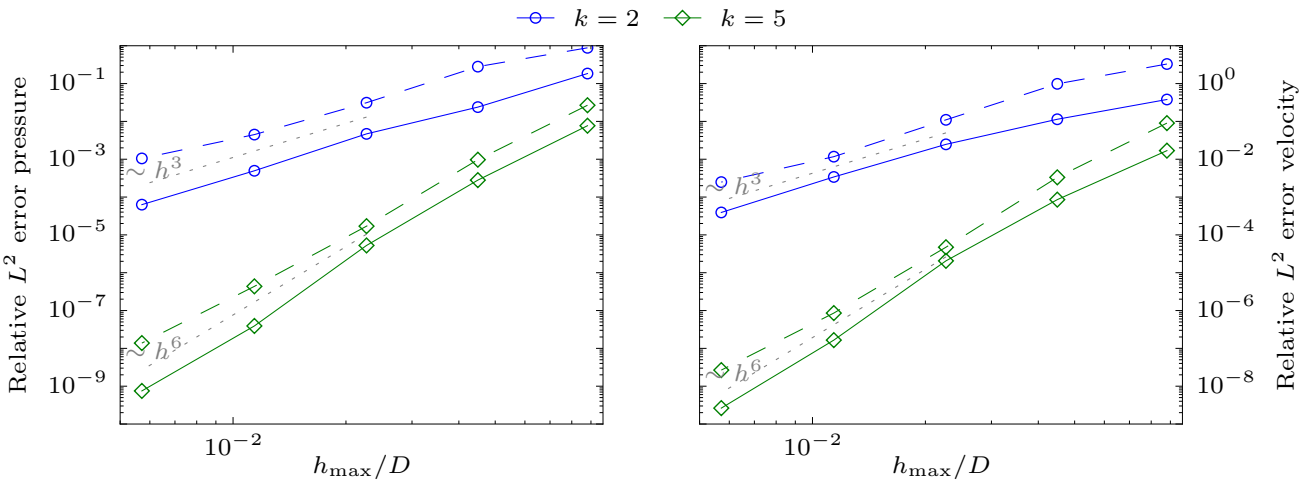

Figure 1: Spatial convergence study for the circular moving gauss pulse test case. The relative L^2 error of the acoustic pressure and acoustic particle velocity are depicted on the left and right, respectively. Lax–Friedrichs are plotted as solid lines ———, LDG fluxes are depicted as dashed lines – – –.

with $\mathcal{P}_k$ being the space of polynomial functions on each element of order k. Eventually, we integrate by parts; at this stage, a numerical flux, denoted by the superscript *, is introduced

$$\left(\boldsymbol{w}_h, \frac{\partial \boldsymbol{u}_h}{\partial t}\right)_{\Omega^e} - \left(\frac{1}{\rho}\nabla\cdot\boldsymbol{w}_h, p_h\right)_{\Omega^e} + \left(\frac{1}{\rho}\boldsymbol{w}_h\cdot\boldsymbol{n}, p_h^*\right)_{\partial\Omega^e} = 0 \quad \forall \boldsymbol{w}_h \in \mathcal{V}_h^u, \tag{6}$$

$$\left(q_h, \frac{\partial p_h}{\partial t}\right)_{\Omega^e} - \left(\rho c^2 \nabla q_h, \boldsymbol{u}_h\right)_{\Omega^e} + \left(\rho c^2 q_h \cdot \boldsymbol{n}, \boldsymbol{u}_h^*\right)_{\partial\Omega^e} = \left(c^2 q_h, f\right)_{\Omega^e} \quad \forall q_h \in \mathcal{V}_h^p. \tag{7}$$

$(\cdot,\cdot)_{\Omega^e}$ and $(\cdot,\cdot)_{\partial\Omega^e}$ denote the inner product, integrated over element volumes and element boundaries, respectively. The definition of the numerical flux is treated in detail within the next section.

Definition of Numerical Flux

Numerical fluxes ensure coupling over element faces between the current element denoted with superscript $-$ and neighboring element denoted with superscript $+$. Thus, on element faces the normal vector $\boldsymbol{n} = \boldsymbol{n}^- = \boldsymbol{n}^+$. For a scalar or vectorial quantity u, the averaging operator is defined as $\{\!\{u\}\!\} = \frac{u^- + u^+}{2}$, while the jump operator is $[u] = u^- - u^+$. It is convenient to introduce a notation for the jump operator multiplied by the normal as $[\![u]\!] = [u]^T \boldsymbol{n}^-$.

Lax–Friedrichs Fluxes

The Lax–Friedrichs fluxes are defined as

$$p_h^* = \{\!\{p_h\}\!\} + \tau\,[\![\boldsymbol{u}_h]\!]\,, \tag{8}$$

$$\boldsymbol{u}_h^* = \{\!\{\boldsymbol{u}_h\}\!\} + \gamma\,[\![p_h]\!]\,. \tag{9}$$

We don't want to manually choose the penalty parameter for each simulation setup but to adjust it depending on the physical quantities. Used penalty parameters are motivated by requiring the Rankine–Hugoniot condition during the derivation of the Riemann solution [9, 6]. This yields $\tau = \frac{\rho c}{2}$ and $\gamma = \frac{1}{2\rho c}$. Note that these penalty parameters are consistent in the context of a dimension analysis which requires $\tau \sim \rho c$ and $\gamma \sim \frac{1}{\rho c}$.

LDG Fluxes

LDG fluxes do not require a penalty parameter

$$p_h^* = \{\!\{p_h\}\!\} - \frac{1-\alpha}{2}\,[p_h]\,, \tag{10}$$

$$\boldsymbol{u}_h^* = \{\!\{\boldsymbol{u}_h\}\!\} + \frac{1-\alpha}{2}\,[\boldsymbol{u}_h]\,. \tag{11}$$

They are written in penalty formulation (motivated by [1, 10]) to be able to choose the upwinding amount easily. These fluxes are used in [13] for the 1D case. The different upwinding directions are critical for stability. With $\alpha \in [0, 2]$ we are able to recover central fluxes with $\alpha = 1$ and monotone upwind fluxes with $\alpha = 0$. Using $\alpha = 2$ leads to monotone upwind fluxes with reversed directions.

Numerical Results

All results within this work are computed with the same polynomial orders for pressure and velocity $k = k_u = k_p$. The timestep size is computed according to the Courant–Friedrichs–Lewy (CFL) condition

$$\Delta t = \frac{\mathrm{Cr}}{k_{\max}^{1.5}} \frac{h_{\min}}{c}. \tag{12}$$

In (12) h denotes the element edge length, and accordingly, $h_{\min}$ is the least element edge length. The superscript 1.5 is motivated by [4]; it originates from the different spacing between Legendre–Gauss–Lobatto nodes which are used as integration points (see also [5]). Within this work, we choose a Courant–Number of $\mathrm{Cr} = 0.05$. In combination with an explicit Runge–Kutta scheme of order 3 we can ensure that instabilities will not arise from the temporal discretization. To evaluate both methods we use a `C++` code based on the finite element library `NGSolve` [12].

Circular Moving Gauss Pulse

We use a benchmark test case with a known analytical solution to compare both methods regarding accuracy and to determine the related convergence behavior; It uses the numerically challenging physical quantities of water, i.e., $\rho = 1000\left[\frac{\mathrm{kg}}{\mathrm{m}^3}\right]$ and $c = 1500\left[\frac{\mathrm{m}}{\mathrm{s}}\right]$. Kronbichler *et al.* [7] used the method of manufactured solution

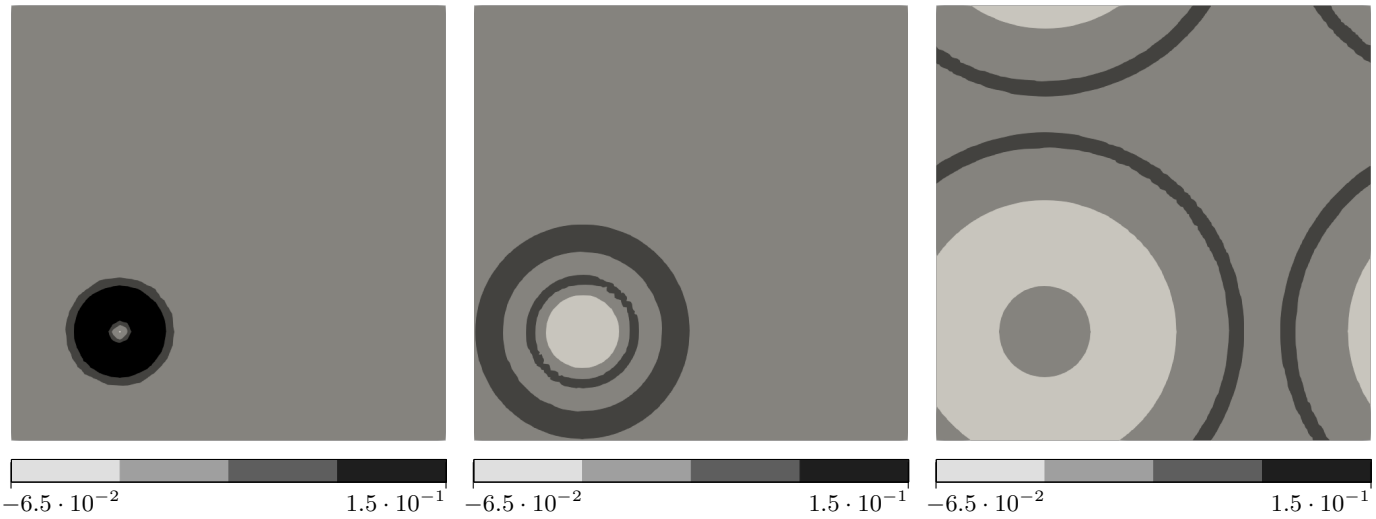

(a) $t = 0\,[\mathrm{s}]$ **(b)** $t = 2 \cdot 10^{-4}\,[\mathrm{s}]$ **(c)** $t = 5 \cdot 10^{-4}\,[\mathrm{s}]$

Figure 2: Acoustic pressure [Pa] in domain treaded with periodic BCs at different times. Results are obtained using the Lax–Friedrichs fluxes.

to generate this test case; acoustic pressure

$$p = \frac{2\xi\alpha l\,(x\cos(\xi t) - y\sin(\xi t))}{\mathrm{e}^{\alpha((x - l\sin(\xi t))^2 + (y - l\cos(\xi t))^2)}}, \tag{13}$$

and acoustic particle velocity

$$\boldsymbol{u} = \frac{-2\alpha\rho^{-1}}{\mathrm{e}^{\alpha((x - l\sin(\xi t))^2 + (y - l\cos(\xi t))^2)}} \begin{pmatrix} l\sin(\xi t) - x \\ l\cos(\xi t) - y \end{pmatrix}, \tag{14}$$

are prescribed. Inserting both in the governing equations (1, 2) yields the right-hand side

$$f = \frac{2\eta l}{c^2 \mathrm{e}^{\eta\left((-l\sin(t\xi)+x)^2 + (-l\cos(t\xi)+y)^2\right)}} \begin{pmatrix} 2c^2 \\ 2\eta l^2 \xi^2 \end{pmatrix} \cdot \begin{pmatrix} 1 - \eta\left(-l\sin(t\xi) + x\right)^2 - \eta\left(-l\cos(t\xi) + y\right)^2 \\ \left(x\cos(t\xi) - y\sin(t\xi)\right)^2 - \frac{x\sin(t\xi) + y\cos(t\xi)}{2\eta l} \end{pmatrix}. \tag{15}$$

Within the simulation we use the same parameters as in [7], i.e. $\eta = 1.6 \cdot 10^{-5}\left[\frac{1}{\mathrm{m}^2}\right], \xi = 4.0 \cdot 10^5\left[\frac{1}{\mathrm{s}}\right]$, and $l = 0.02\,[\mathrm{m}]$. Errors are evaluated at $T = 1.5 \cdot 10^{-5}\,[\mathrm{s}]$ on a circular domain of diameter $D = 0.04\,[\mathrm{m}]$; at this time the moving pulse nearly completed one round. We treat all boundaries as $\partial\Omega_u$ (cf. Eq. (3)) with $\boldsymbol{g}_u$ from Eq. (14). The corresponding convergence plot is depicted in Fig. 1. Indeed both methods yield optimal spatial convergence rates for pressure and velocity of $k+1$. However, the LDG fluxes are subject to more significant numerical errors than the Lax–Friedrichs fluxes. Note that this holds for all tested orders $k = 1$ to $k = 7$; we only show this for $k = 2$ and $k = 5$ to keep the picture intelligible.

Periodic Box

Thoroughly testing both equations for different test cases, we encounter instabilities for the LDG method, whereas the Lax–Friedrichs fluxes remain stable. Described instabilities are independent of the choice of α and mainly occur if first-order absorbing BCs or sound hard BCs are applied. A computational domain with periodic boundaries is considered within the following to show that instabilities do not originate from mentioned BCs alone. The pressure is initialized with a Gauss pulse centered around $\boldsymbol{x} = (0, 0)^T$ in a domain of size $\Omega = \left[-\frac{L}{4}, \frac{3L}{4}\right]^d$, with $L = 2\,[\mathrm{m}]$

$$p = \mathrm{e}^{-50(x^2+y^2)} - \mathrm{e}^{-100(x^2+y^2)}, \tag{16}$$

$$\boldsymbol{u} = \boldsymbol{0}. \tag{17}$$

Again we use the material properties of water. Provided results are computed with orders $k = 1$ and 8192 triangular elements. The expected results are obtained with the Lax–Friedrichs fluxes; the pressure results are depicted in Fig. 2. The results obtained at $t = 5 \cdot 10^{-4}\,[\mathrm{s}]$ with the LDG method are plotted in Fig. 3 for different α. Since the stability mechanism is based on upwinding, we show results for small α to ensure a dominat upwinding part. Note, however that we experience the same instabilities for larger α. We can see in Fig. 3 that the LDG scheme gets instable, independent of the choice of α. In the case of periodic boundary conditions, we were able to resolve this issue by using more degrees of freedom. This is not the case for first order absorbing and sound hard BCs.

Conclusion

Within this work, we compared numerical fluxes for DG discretizations of the acoustic conservation laws regarding accuracy and stability. We numerically showed that both numerical fluxes are subject to optimal spatial rates of convergence; using the Lax–Friedrichs fluxes yields more accurate results compared to LDG fluxes, though. Using a different numerical test case, we showed that employing the LDG fluxes might lead to instabilities whereas employing Lax–Friedrichs fluxes yields a stable scheme. Additional stabilization techniques are required for the LDG fluxes in 2D, and consequently, Lax–Friedrichs fluxes should be preferred over LDG fluxes, if used without additional stabilization, for the solution of

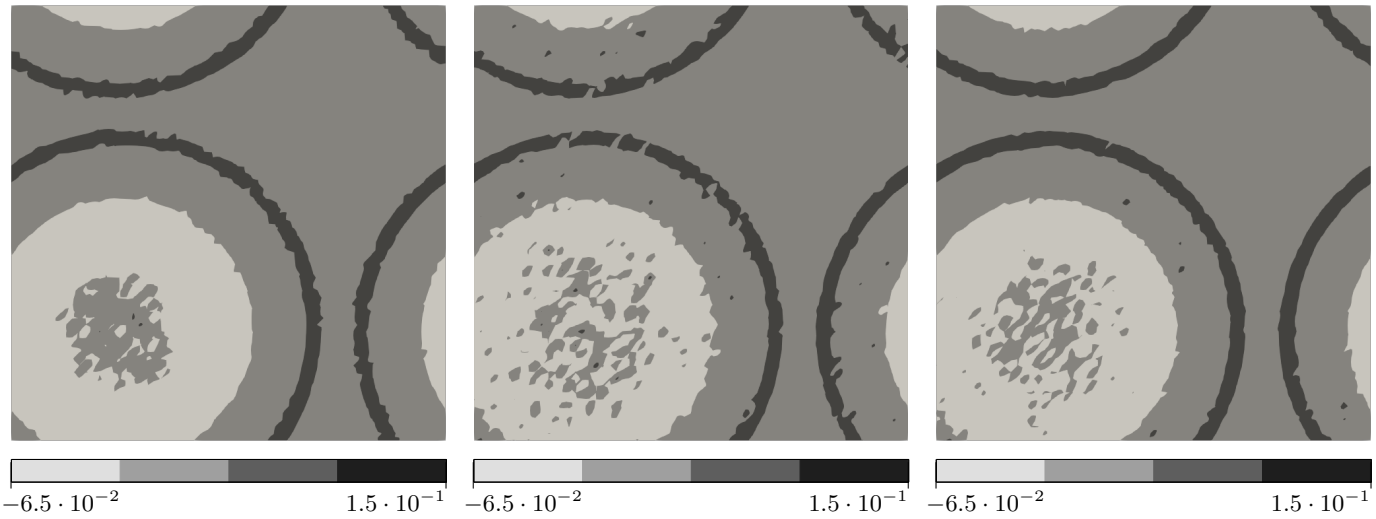

(a) $\alpha = 0$ **(b)** $\alpha = 0.25$ **(c)** $\alpha = 0.5$

Figure 3: Acoustic pressure [Pa] in domain treaded with periodic BCs at $t = 5 \cdot 10^{-4}$ [s]. Results are obtained using the LDG fluxes with different α.

the acoustic conservation laws.

Acknowledgement

Special thanks to Lukas Kogler for several invaluable discussions on the implementational aspects of `NGSolve` [12].

This project has received funding from the European Union's Framework Programme for Research and Innovation Horizon 2020 (2014-2020) under the Marie Skłodowska–Curie Grant Agreement No. [812719].

Bibliography

[1] F. Brezzi, L. D. Marini, and E. Süli. "Discontinuous Galerkin methods for first-order hyperbolic problems." In: *Mathematical Models and Methods in Applied Sciences* 14.12 (2004), pp. 1893–1903. DOI: 10.1142/s0218202504003866.

[2] Gary Cohen and Sandrine Fauqueux. "Mixed finite elements with mass-lumping for the transient wave equation." In: *Journal of Computational Acoustics* 08.01 (2000), pp. 171–188. DOI: 10.1142/s0218396x0000011x.

[3] Gary C. Cohen. *Higher-Order Numerical Methods for Transient Wave Equations*. Springer Berlin Heidelberg, 2002. DOI: 10.1007/978-3-662-04823-8.

[4] Niklas Fehn, Wolfgang A. Wall, and Martin Kronbichler. "Robust and efficient discontinuous Galerkin methods for under-resolved turbulent incompressible flows." In: *Journal of Computational Physics* 372 (2018), pp. 667–693. ISSN: 0021-9991. DOI: 10.1016/j.jcp.2018.06.037.

[5] Jan S. Hesthaven and Tim Warburton. *Nodal Discontinuous Galerkin Methods*. Springer, New York, NY, 1, 2008. ISBN: 978-0-387-72065-4. DOI: 10.1007/978-0-387-72067-8.

[6] Marlis Hochbruck et al. "Efficient time integration for discontinuous Galerkin approximations of linear wave equations." In: *ZAMM - Journal of Applied Mathematics and Mechanics / Zeitschrift für Angewandte Mathematik und Mechanik* 95.3 (2014), pp. 237–259. DOI: 10.1002/zamm.201300306.

[7] M. Kronbichler et al. "Comparison of implicit and explicit hybridizable discontinuous Galerkin methods for the acoustic wave equation." In: *International Journal for Numerical Methods in Engineering* 106.9 (2016), pp. 712–739. DOI: 10.1002/nme.5137.

[8] Martin Kronbichler and Katharina Kormann. "Fast matrix-free evaluation of discontinuous Galerkin finite element operators." In: *ACM Trans. Math. Softw.* 45.3 (2019). ISSN: 0098-3500. DOI: 10.1145/3325864.

[9] Randall J. LeVeque. "Finite Volume Methods for Hyperbolic Problems." In: (2002). DOI: 10.1017/cbo9780511791253.

[10] Xiong Meng, Chi-Wang Shu, and Boying Wu. "Optimal error estimates for discontinuous Galerkin methods based on upwind-biased fluxes for linear hyperbolic equations." In: *Mathematics of Computation* 85.299 (2015), pp. 1225–1261. DOI: 10.1090/mcom/3022.

[11] N.C. Nguyen, J. Peraire, and B. Cockburn. "High-order implicit hybridizable discontinuous Galerkin methods for acoustics and elastodynamics." In: *Journal of Computational Physics* 230.10 (2011), pp. 3695–3718. ISSN: 0021-9991. DOI: https://doi.org/10.1016/j.jcp.2011.01.035.

[12] Joachim Schöberl. *C++11 Implementation of Finite Elements in NGSolve*. 2014.

[13] Rongpei Zhang et al. "The local discontinuous Galerkin method with generalized alternating flux applied to the second-order wave equations." In: *Complexity* 2020 (2020), pp. 1–9. DOI: 10.1155/2020/8464153.